Climate Dynamics (2025) 63:153
https://doi.org/10.1007/s00382-025-07647-2

ORIGINAL ARTICLE

Summer precipitation responses to CO_2 removal scenario over the transitional climate zone in East Asia and the driving mechanisms

Xiaoyun Su[1,3] · Lin Wang[1,4] · Gang Huang[1,2,3] · Ting Wang[5] · Jinling Piao[1] · Qiulin Wang[6]

Received: 8 October 2024 / Accepted: 3 March 2025

Abstract
The Transitional Climate Zone (TCZ) in East Asia represents a critical region where monsoon and non-monsoon climates interface, making it highly vulnerable to climate change. While TCZ precipitation changes under global warming have been well-studied, its response to CO_2 removal (CDR) remains poorly understood. This study investigates TCZ summer precipitation changes under an idealized CDR scenario and reveals a region-wide decrease during CO_2 ramp-down, with the strongest signals in the northeastern regions. Notably, the precipitation response under equal levels of warming or CO_2 forcing demonstrates clear asymmetry, characterized by drying during the CO_2 ramp-down rather than the ramp-up. Moisture budget analysis indicates that the reduction in precipitation during the CO_2 ramp-down period is closely associated with the divergence of vertically integrated atmospheric moisture flux. The divergence is primarily driven by dynamic processes (36.4%) rather than thermodynamic effects (5.2%). Quantification of moisture transport shows a net moisture output from the TCZ, with 78.6% attributed to the meridional monsoon moisture and 18.3% to the zonal westerlies. Further analysis of the East Asia Summer Monsoon (EASM) characteristics demonstrates that during CO_2 ramp-down, the monsoon system exhibits a weakened intensity, a southward retreat of its northern boundary, and a shortened duration with delayed onset and earlier withdrawal. Among these factors, the southward shift of the northern boundary has the greatest impact on the precipitation reduction, followed by the changes in monsoon duration. These findings suggest that CDR, despite its intended role in mitigating global warming, may enhance drying risks in the TCZ through altered atmospheric circulation patterns.

Keywords Carbon dioxide removal · Transitional climate zone · Summer precipitation · Moisture budget · East Asia summer monsoon

1 Introduction

The Transition Climate Zone (TCZ) in East Asia, situated between monsoon and non-monsoon regions, as well as between humid and arid areas, is characterized by a northeast-southwest oriented belt (Tang et al. 2006; Piao et al. 2023; Chen et al. 2024). The TCZ is characterized by distinct climate and biome gradients, making it an extremely delicate ecosystem that is particularly susceptible to climate change and prone to natural disasters. Any deficiency or

✉ Lin Wang
linwang@mail.iap.ac.cn; wang_lin@mail.iap.ac.cn

✉ Gang Huang
hg@mail.iap.ac.cn

[1] National Key Laboratory of Earth System Numerical Modeling and Application, Institute of Atmospheric Physics, Chinese Academy of Sciences, Beijing 100029, China

[2] Laboratory for Regional Oceanography and Numerical Modeling, Qingdao National Laboratory for Marine Science and Technology, Qingdao 266237, China

[3] College of Earth and Planetary Sciences, University of Chinese Academy of Sciences, Beijing 100049, China

[4] CAS Key Laboratory of Regional Climate-Environment for Temperate East Asia, Institute of Atmospheric Physics, Chinese Academy of Sciences, Beijing 100029, China

[5] Carbon Neutrality Research Center, Institute of Atmospheric Physics, Chinese Academy of Sciences, Beijing 100029, China

[6] Hangzhou Meteorological Bureau, Hangzhou 310051, China

Published online: 11 March 2025

surplus in precipitation can have significant consequences for agriculture, animal husbandry, and socioeconomics. For example, in the summer of 2014, seven provinces in northern China experienced severe drought, with some areas suffering the most intense drought in 60 years (Wang and He 2015). Conversely, the summer of 2021 saw an exceptionally intense rainy season in northern China, with rainfall levels doubling the average for that time of year, and record-breaking hourly precipitation (201.9 mm) recorded at Zhengzhou station (Zhou and Lu 2024). Consequently, the TCZ is also a disaster-prone belt and a farming-grazing ecotone (Neilson 1993; Shi 1996; Lu and Jia 2013). Due to its unique geographical location and climate characteristics, it has become increasingly urgent to enhance our understanding of future climate changes in the TCZ.

The TCZ is shaped by the interannual fluctuations of the northern boundary of the East Asia summer monsoon (EASM). Previous studies provide different definitions of the northern boundary, which can be roughly classified into the following two types: one focuses on the air mass interaction between warm-humid air from lower latitudes and dry-cold air from higher latitudes, using variables such as pseudo-equivalent potential temperature, specific humidity, precipitable water, moisture transport flux, and wind fields to define the northern boundary of EASM. (Tu and Huang 1944; Wang et al. 1999; Wu et al. 2005; Ha et al. 2020). The other is from the precipitation perspective, focusing on the seasonal northward advance of the EASM precipitation (Wang and LinHo 2002; Chen et al. 2018; Zhao et al. 2019c).

Due to its unique geographical location, the dry-wet changes of the TCZ are quite complex and influenced by both low and mid-high latitude systems. Numerous studies have investigated the characteristics and mechanisms of precipitation changes in the TCZ across interannual, interdecadal, and long-term trends. On an interannual scale, factors influencing summer precipitation in the TCZ include local climate systems (e.g., EASM and mid-latitude westerlies), remote oceanic forcings (e.g., the North Atlantic Oscillation (NAO), Atlantic and Pacific sea surface temperature (SST) anomalies), and atmospheric teleconnection modes (e.g., the Polar-Eurasian (PEU), the Circumglobal teleconnection (CGT), and Eurasian teleconnection (EU), which modulated atmospheric vertical motion and moisture supply over the TCZ (Lin 2014; Lin and Wang 2016; Bueh et al. 2016; Zhao et al. 2019a, 2020; Wang et al. 2022a, 2023b). The late 1990s saw the formation of a "Silk Road pattern" due to the combined influence of the Atlantic Multidecadal Oscillation (AMO) and phase shifts in the Pacific Decadal Oscillation (PDO), resulting in a 15.7% decrease in TCZ summer precipitation and a significant increase in drought frequency and intensity (Chen and Sun 2015; Piao et al. 2017, 2021a).

In recent decades, under the global warming induced by greenhouse gas emissions, North China has exhibited the most significant drying trend in China, with the TCZ showing pronounced signals (Ma and Fu 2006; Chen and Sun 2015; Wang et al. 2017, 2023a; Chen et al. 2019, 2024). Different climate models consistently predict that, if global warming continues, the northern boundary will shift significantly northwestward, and precipitation in the TCZ will increase, with the strongest signals in summer. (Piao et al. 2021b, 2022; Wang et al. 2022b; Chen et al. 2023). However, the uncertainty of internal atmospheric variability remains a concern for these projections.

In summary, current studies on TCZ precipitation and driving factors primarily focus on present climate and global warming scenarios. However, the 2015 Paris Agreement proposed a target of "holding the increase in the global average temperature to well below 2°C above pre-industrial (PI) levels and pursuing efforts to limit the temperature increase to 1.5°C above PI". According to the World Meteorological Organization's (WMO) State of the Global Climate 2023 report, the global near-surface temperature has already increased by approximately 1.45 °C above the 1850–1900 average, with CO_2 concentrations increasing by 50%. These developments underscore the urgency of reducing carbon emissions and enhancing carbon sequestration. However, the scientific community lacks consensus on the impact of CO_2 removal (CDR) on climate systems, prompting initiatives like the CDR Model Intercomparison Program (Keller et al. 2018). Studies suggest that the climate responses and dynamics of CDR on precipitation will differ significantly from past climate patterns, particularly in regions like East Asia (Long et al. 2020; Hou et al. 2021; Huang et al. 2022; Zhou et al. 2022). Global precipitation continues to increase after the CO_2 peak due to the large thermal inertia of the ocean and the weakened influence of CO_2 radiative forcing. Even after CO_2 decreases and stabilizes, both oceanic and terrestrial precipitation do not return to their PI levels (Wu et al. 2015; Sun et al. 2021; Yeh et al. 2021; Cao et al. 2023; Su et al. 2024). In East Asia, Song et al. (2021) and Jo et al. (2022) have studied the asymmetry in mean and extreme precipitation frequencies during CO_2 ramp-up and ramp-down periods, which is caused by the persistence of El Niño-like warming in the equatorial Pacific Ocean after CO_2 begins to decrease. Furthermore, Sun et al. (2021) reported that with symmetric CO_2 concentrations, the EASM rainband moves northward with an earlier onset, delayed withdrawal, and longer duration.

While substantial research has focused on precipitation changes and their drivers in the TCZ under global warming, little is known about how these changes will manifest

under future CDR scenario. Several key questions remain unanswered: What are the spatial and temporal characteristics of TCZ summer precipitation changes under CDR scenario? To what extent are these changes influenced by the EASM compared to the mid-latitude westerlies, and which aspects of the EASM, including intensity, northern boundary position, and influence time have the greatest impact on TCZ precipitation? Furthermore, how do the TCZ responses differ between CO_2 ramp-down and ramp-up periods under the same warming levels? This study aims to address these questions by investigating TCZ summer precipitation responses to an idealized CDR scenario. Through comprehensive moisture budget analysis and examination of monsoon system changes, we seek to understand the mechanisms governing TCZ summer precipitation changes during CDR, with implications for regional climate adaptation under future carbon neutrality scenarios. The paper is structured as follows: Sect. 2 describes the data and methods employed, Sect. 3 presents the results, and Sect. 4 provides the discussion and conclusions.

2 Data and methods

2.1 Data

In this study, the observation and reanalysis datasets employed include: (1) daily precipitation data from the National Meteorological Information Center, with a horizontal resolution of 0.5° × 0.5° (Xu et al. 2020); (2) monthly precipitation data from the Climatic Research Unit (CRU) at a 0.5° × 0.5° resolution (Harris et al. 2020); (3) monthly precipitation reconstruction data over land (PREC/L) from the National Oceanic and Atmospheric Administration (NOAA) with a horizontal resolution of 1° × 1°(Chen et al. 2002). All the above datasets cover a common period of 1979–2014.

The model data are from three experiments conducted under the Coupled Model Intercomparison Project 6 (CMIP6), which are the *piControl* experiment, the *1pctCO*$_2$ experiment, and the *1pctCO*$_2$*-cdr* experiment (Keller et al. 2018). The *1pctCO*$_2$ experiment starts from the 1850 state with an atmospheric CO_2 concentration of 284.7 ppm and gradually increases by 1% per year until reaching four times that of the *piControl* experiment (1138.8 ppm; run for 140 years). Then, it gradually decreases at the same rate back to the *piControl* level. After that, the CO_2 concentration is kept at 284.7 ppm for as long as possible, but here only the subsequent 60 years are selected for analysis. It is noteworthy that the only externally imposed forcing is CO_2 concentration, while all other forcings remain fixed at 1850 levels.

To date, 9 models have participated in all three CMIP6 experiments required for this study (Table S1). According to the Taylor diagram shown in Fig. S1, the 9 models effectively reproduce the precipitation patterns from reanalysis data, with the multi-model ensemble mean (MME) performing better than any individual model. The spatial correlation coefficients for individual models all exceed 0.6, while the MME reaches approximately 0.84. All model output data are interpolated onto a 1° × 1° grid. Monthly precipitation, specific humidity, horizontal wind, and surface pressure are used in this study. The ensemble spread is defined as 1 standard deviation among the 9 models, and the results are considered robust if more than 2/3 of the models exhibit the same sign as the MME. To minimize the influence of interannual fluctuations, a 21-year running mean was applied to filter the data.

2.2 Definition of the TCZ region

According to Chen et al. (2018), the northern boundary of the EASM is defined as the 2 mm day^{-1} precipitation isoline during the boreal summer (i.e., May-September-averaged). Therefore, based on this definition, using PREC/L, CRU, and CMA precipitation data with a 7-year moving average applied, the EASM northern boundaries are derived for the years 1979–2014. Consequently, the region where these boundaries overlap is referred to as the TCZ region, which appears as a southwest-northeast oriented belt that includes parts of northern and northeastern China (red box in Fig. 1). The TCZ region defined in this study is consistent with findings from previous studies using different data sources and definitions (Zhao et al. 2019b; Wang et al. 2021; Piao et al. 2022), indicating the robustness and reliability of this region definition.

2.3 Moisture budget

According to previous studies (Trenberth and Guillemot 1995; Simmonds et al. 1999), the moisture budget equation can be expressed as:

$$\frac{\partial \mathrm{W}}{\partial \mathrm{t}} + \nabla \cdot \mathrm{Q} = \mathrm{E} - \mathrm{P}, \tag{1}$$

where W represents precipitable water, while E and P denote evaporation and precipitation, respectively. Q refers to the vertically integrated atmospheric moisture flux, which is expressed as:

$$Q = -\frac{1}{g}\int_{P_s}^{P_t} V q dp. \tag{2}$$

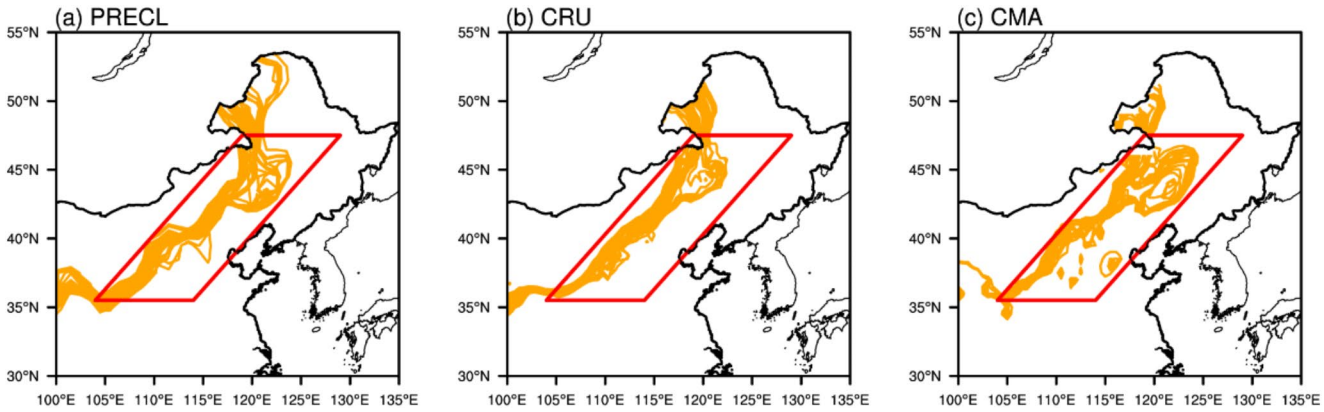

Fig. 1 The 2 mm day^{-1} isochrones in the 7-year running mean precipitation in boreal summer (i.e., May-September-averaged) from 1979 to 2014 (orange lines). The red boxes represent the TCZ region

Here, P_t and P_s denote the upper-level pressure and surface pressure; g is the acceleration of gravity; V is horizontal wind; and q is specific humidity. P_t is set to 100 hPa here since water vapor is mostly concentrated below this level.

By averaging Eq. (1) over the summer (June-August), the first term can be neglected, so the divergence of the vertically integrated atmospheric moisture flux determines the precipitation minus evaporation (P-E) exchange with the surface. The expression becomes:

$$\bar{P} - \bar{E} = -\nabla \cdot \bar{Q} = \frac{1}{g}\nabla \cdot \int_{P_s}^{P_t} \overline{Vq} dp. \tag{3}$$

Overbars indicate summer means.

For a certain variable X, it can be expressed as the climatological mean X_{cli} plus the anomaly relative to the climatological mean X', as shown in the following form:

$$X = X_{cli} + X', \tag{4}$$

Therefore, according to Eq. (3), the P-E anomaly can be sequentially decomposed into the dynamic (DY) term related to the wind field anomaly, the thermodynamic (TH) term related to the specific humidity anomaly, and the nonlinear (NL) term, as shown below:

$$\begin{aligned}\overline{P'} - \overline{E'} =& \frac{1}{g}\nabla \cdot \int_{P_s}^{P_t} q_{cli}\overline{V'} dp + \frac{1}{g}\nabla \cdot \int_{P_s}^{P_t} \overline{q'} V_{cli} dp \\ &+ \frac{1}{g}\nabla \cdot \int_{P_s}^{P_t} \overline{q'V'} dp.\end{aligned} \tag{5}$$

2.4 EASM activity index

2.4.1 EASM intensity index

Previous studies have defined a large number of indices to describe the intensity of the EASM (Wang and Fan 1999; Wang 2002; Wang et al. 2008; Zhao et al. 2015). According to Wang et al. (2008), among 25 different indices, the shear vorticity index defined by Wang and Fan (1999) shows the strongest correlation (-0.97) with the leading principal component obtained from a multivariate empirical orthogonal function (MV-EOF) analysis of the EASM. Therefore, to measure the changes in EASM intensity, we adopt the negative of the Wang and Fan (1999) index (WFI):

$$\begin{aligned}WFI =& U_{850}\left(22.5^\circ - 32.5^\circ N, 110^\circ - 140^\circ E\right) \\ &- U_{850}\left(5^\circ - 15^\circ N, 90^\circ - 130^\circ E\right),\end{aligned} \tag{6}$$

where U_{850} represents the 850 hPa zonal wind.

2.4.2 EASM Northern boundary index

Similar to Sect. 2.2, the 2 mm day^{-1} precipitation isoline is used to represent the northern boundary of the EASM, and the mean latitude of this isoline can serve as the EASM northern boundary index. First, the EASM northern boundaries in climate models exhibit systematic biases from observations. As shown in Fig. S2a, almost all models simulate a northward- shifted boundary compared to the observation. Moreover, when CO_2 reaches its peaks, the boundaries are projected to shift even further northward (Fig. S2b), resulting in incomplete boundary representation in the east part. Given these model characteristics and following Piao et al. (2023), who demonstrated a strong correlation (r=0.81) between the western portion (100°E-110°E) and the full extent (100°E-120°E) of the boundary in representing its variability, we use the western section to represent the

EASM northern boundary. Additionally, since our focus is primarily on the relative movement of the northern boundary rather than its absolute position, the western section (average latitude between 100°E and 110°E) provides a reliable metric for tracking boundary changes throughout the CO_2 evolution.

2.4.3 EASM influence time

Following previous studies (Qian and Qin 2008; Wang et al. 2021), we adopt the 4 mm day^{-1} precipitation threshold as the criterion to determine whether the EASM influences the TCZ. To eliminate the influence of high-frequency oscillations, we adopt the method used by Wang et al. (2021) to filter the daily precipitation time series, thereby obtaining a smoother precipitation sequence. The monsoon rainy season onset (MRO, units: Day of year, DOY) and retreat (MRR, units: DOY) in the TCZ region are defined as the first and last dates when the filtered daily precipitation reaches 4 mm in the boreal summer (May-September), respectively. The monsoon rainy duration (MRD) is then calculated as the period between onset and retreat (MRD = MRR - MRO + 1). This definition is applied to each segment of the TCZ to characterize the temporal evolution of monsoon influence. An example of the MRO, MRR, and MRD definitions of 114°E-119°E and 37.5°N in 1981 is provided in Fig. S3. Daily precipitation data is necessary to determine the onset, retreat, and duration of the EASM's influence on the TCZ region. Among the 9 models, CAS-ESM2-0 did not output this data, so the mean of the remaining 8 models is used for calculation.

3 Result

3.1 Spatial and Temporal changes of summer precipitation

Numerous studies have examined global precipitation responses to idealized CO_2 concentrations (Wu et al. 2015; Sun et al. 2021; Yeh et al. 2021; Cao et al. 2023). However, we find that the TCZ experiences more significant changes in summer precipitation compared to both the global average (Fig. 2a) and its southern monsoon-dominated region (Fig. S4). This enhanced sensitivity can be attributed to the TCZ's characteristic sub-humid to semi-arid climate, where relatively low baseline precipitation makes percentage changes more pronounced in response to external forcing. This highlights the TCZ's particular vulnerability to climate change compared to other regions. During the CO_2 ramp-up period, TCZ summer precipitation increases by 15% (Fig. 2a), remaining elevated for ~20 years post-CO_2 peak. When CO_2 returns to pre-industrial levels, precipitation also nearly returns to its original state (Fig. S5). Spatially, the TCZ exhibits widespread wetting during ramp-up (Fig. S6a) and drying during ramp-down (Fig. 2b). These changes are robust throughout the TCZ, with areas approximately east of 115°E exhibiting more pronounced shifts.

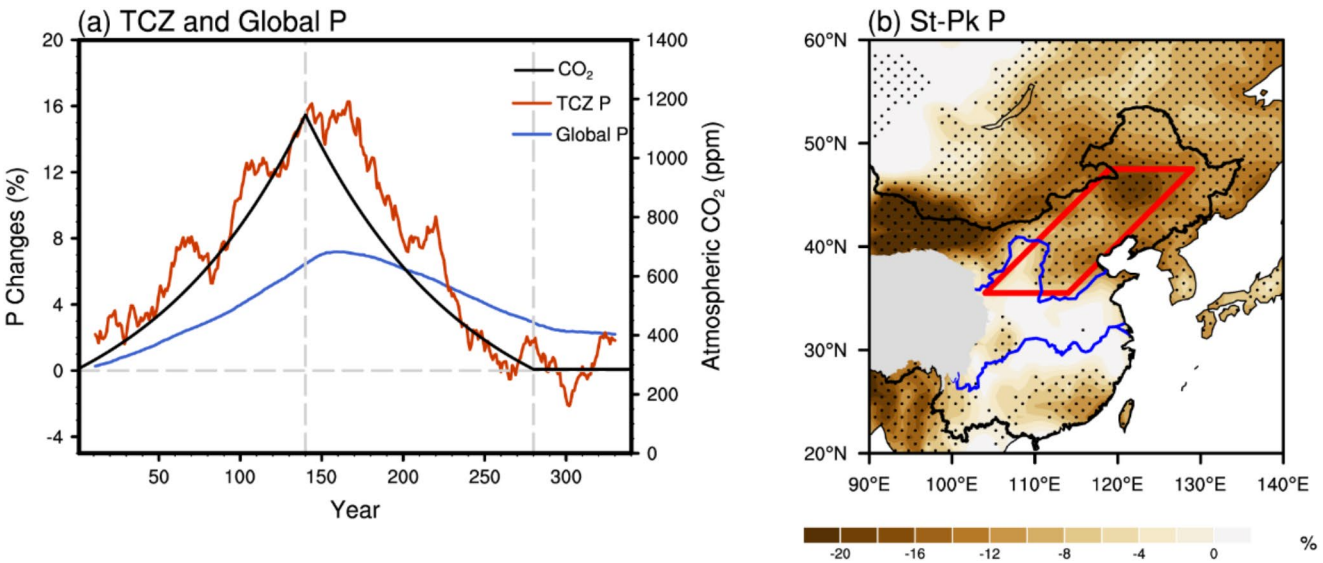

Fig. 2 Temporal evolution and spatial pattern of the TCZ summer precipitation response during the CO_2 ramp-up, ramp-down, and stabilization periods. (**a**) The atmospheric CO_2 concentration (black) and the 21-year running mean of summer precipitation changes in global (blue) and TCZ (red) mean during the CO_2 ramp-up, ramp-down, and stabilization periods relative to the PI levels. The dashed vertical lines indicate the years of CO_2 peak (year 140) and stabilization (year 280). (**b**) The spatial pattern showing the difference between the CO_2 stabilization (St, years 281–340) and peak (Pk, years 131–150) periods. The stippling in (**b**) denotes areas where at least 2/3 of models agree on the sign of the MME change. The TCZ region is highlighted by the red box

3.2 Moisture budget

To unravel the causes behind summer precipitation changes in the TCZ region, we diagnose the moisture budget (Fig. 3). According to the moisture budget equation (Eq. (3)), the summer P-E is balanced by the divergence of the vertically integrated moisture flux, with a correlation coefficient of 0.67 during the CO_2 (Fig. 3a). As shown in Fig. 3a, during the CO_2 ramp-up period, the TCZ experiences an increase in summer P-E. However, P-E decreases after CO_2 peaks, gradually returning to PI levels around the 230th year and stabilizing thereafter. Spatially, during the CO_2 removal phase, there is a general decrease in P-E across the TCZ, with the northeastern areas showing the most pronounced drying (Fig. 3b). During the CO_2 ramp-down period, the spatial pattern over the TCZ is characterized by a divergence

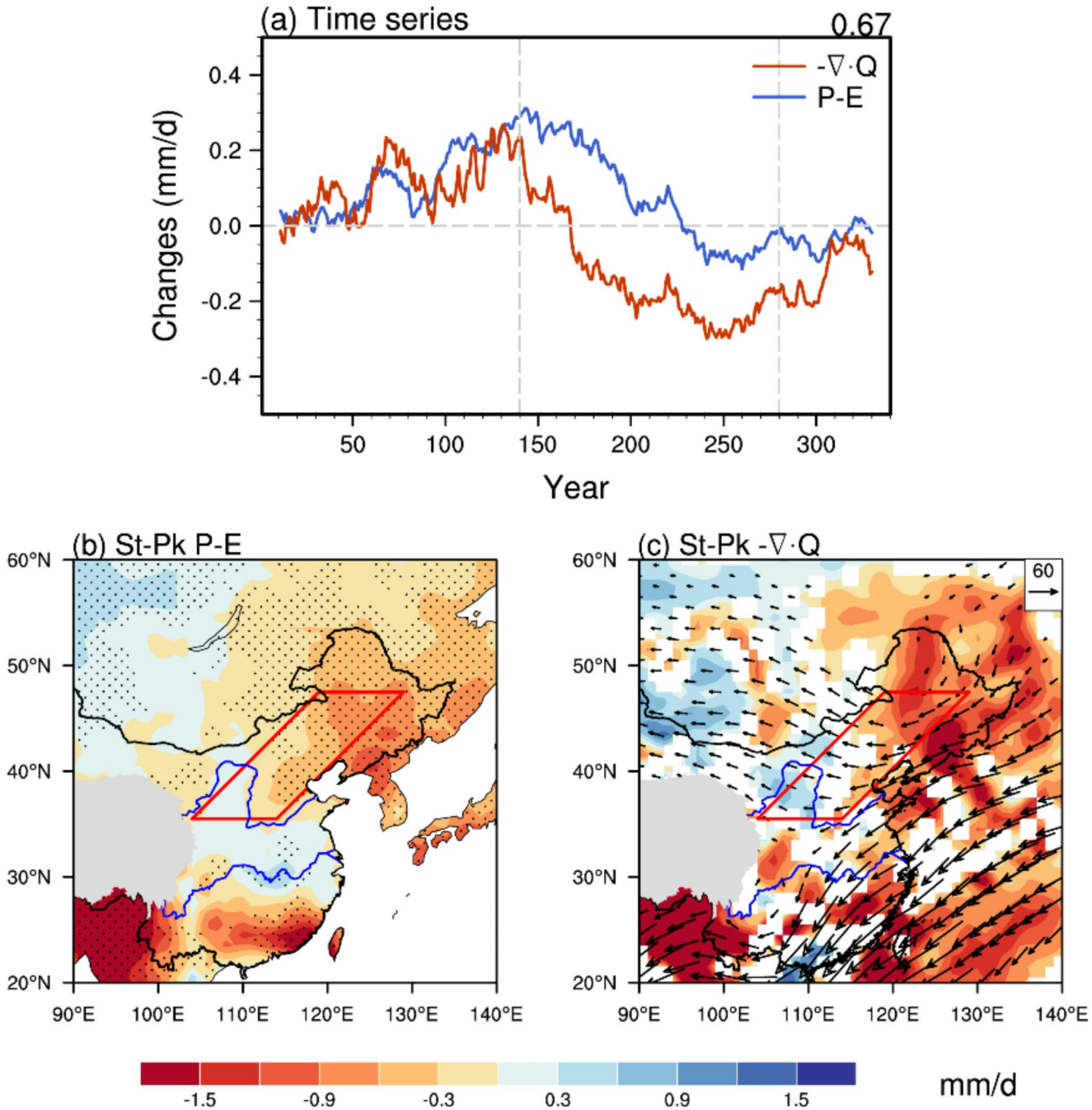

Fig. 3 (**a**) The 21-year running mean changes of P-E (blue) and the convergence of vertically integrated moisture flux (red). Spatial differences of (**b**) P-E, (**c**) the vertically integrated moisture flux (vectors, unit: $kg \cdot m^{-1} \cdot s^{-1}$) and its divergence (shadings) between the CO_2 St and Pk periods (unit: $mm \cdot day^{-1}$). The stippling and red box are the same as in Fig. 2b

of vertically integrated atmospheric moisture flux (Fig. 3c), leading to a reduction in P-E. Notably, anomalous northeasterly and easterly moisture transport prevails throughout the TCZ, indicating a weakening of the westerlies and summer monsoon circulation in this region.

The westerlies and monsoon are the primary sources of moisture transported into the TCZ (Wang et al. 2023b; Ren et al. 2024). To examine the relative contributions of these two components during the CO_2 ramp-down period, we calculate the changes in moisture transport into the TCZ through each boundary (Fig. 4a, Fig. S7). In summer, the TCZ experiences a net moisture output of 0.16×10^7 kg·s^{-1}, composed of a zonal net input of 2.32×10^7 kg·s^{-1} and a meridional net output of 2.48×10^7 kg·s^{-1}. Given that zonal moisture transport primarily reflects westerly influence and meridional transport represents monsoon circulation, we conducted regression analysis of these components against the vertically integrated moisture flux divergence over the TCZ (Fig. 4b, c). The spatial pattern reveals that zonal moisture transport mainly reduces moisture flux in

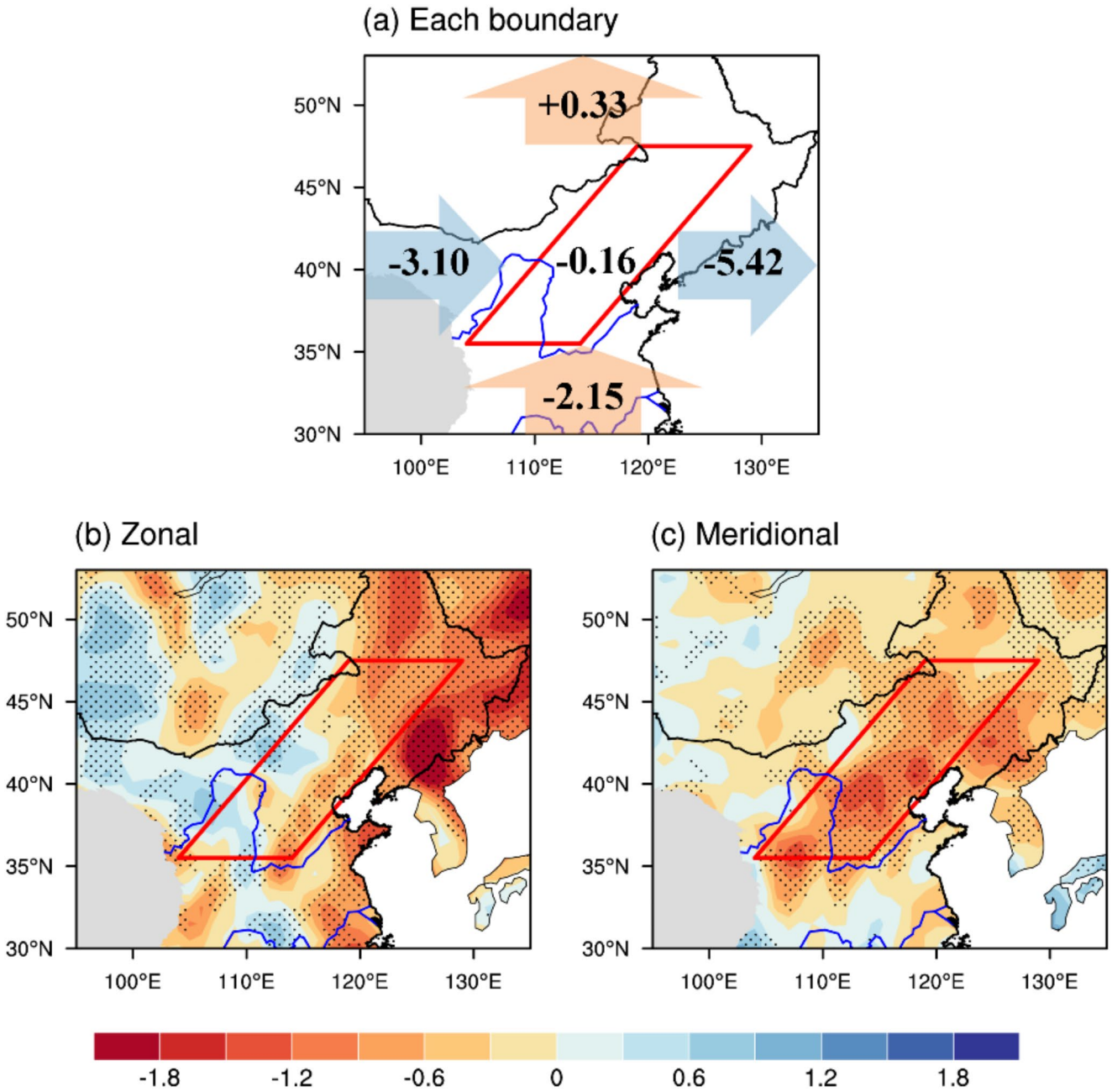

Fig. 4 (**a**) Moisture transport differences (unit: 10^7 kg·s^{-1}) across each boundary of the TCZ during summer between the CO_2 stabilization (St) and peak (Pk) periods. (**b**, **c**) Regression coefficients of zonal and meridional net moisture transport against the vertically integrated moisture flux divergence (unit: 10^{-13} m^{-2}). The stippling and red box are the same as in Fig. 2b

the eastern TCZ, while meridional transport causes a more uniform reduction across the entire region. Together, they result in more pronounced moisture decreases in the region east of 115°E (Fig. 3b). Overall, meridional transport has a greater impact on TCZ moisture flux, with coefficients of determination of 18.3% and 78.6% for zonal and meridional transport, respectively, underscoring the dominant role of monsoon moisture compared to westerly moisture in driving summer net moisture budget changes.

To further investigate the drivers of changes in the vertically integrated atmospheric moisture flux divergence, a decomposition into dynamic, thermodynamic, and nonlinear components is performed (Eq. (5)). Figure 5 shows their temporal and spatial variations. A multiple regression analysis is also conducted to quantify the association between these components and the P-E in the TCZ, with the corresponding coefficients of determination displayed in Fig. 6. The dynamic component, related to anomalies in the wind field, contributes the most, with the explained variance amounting to 36.4%. During the CO_2 ramp-down period, the dynamic component consistently reduces P-E input across the TCZ with good robustness. In comparison, the thermodynamic component, associated with specific humidity anomalies, exhibits a much smaller contribution with the explained variance of 5.2%, along with minor amplitudes and poor robustness in the region. In addition, the contributions and variations of the nonlinear component are also negligible.

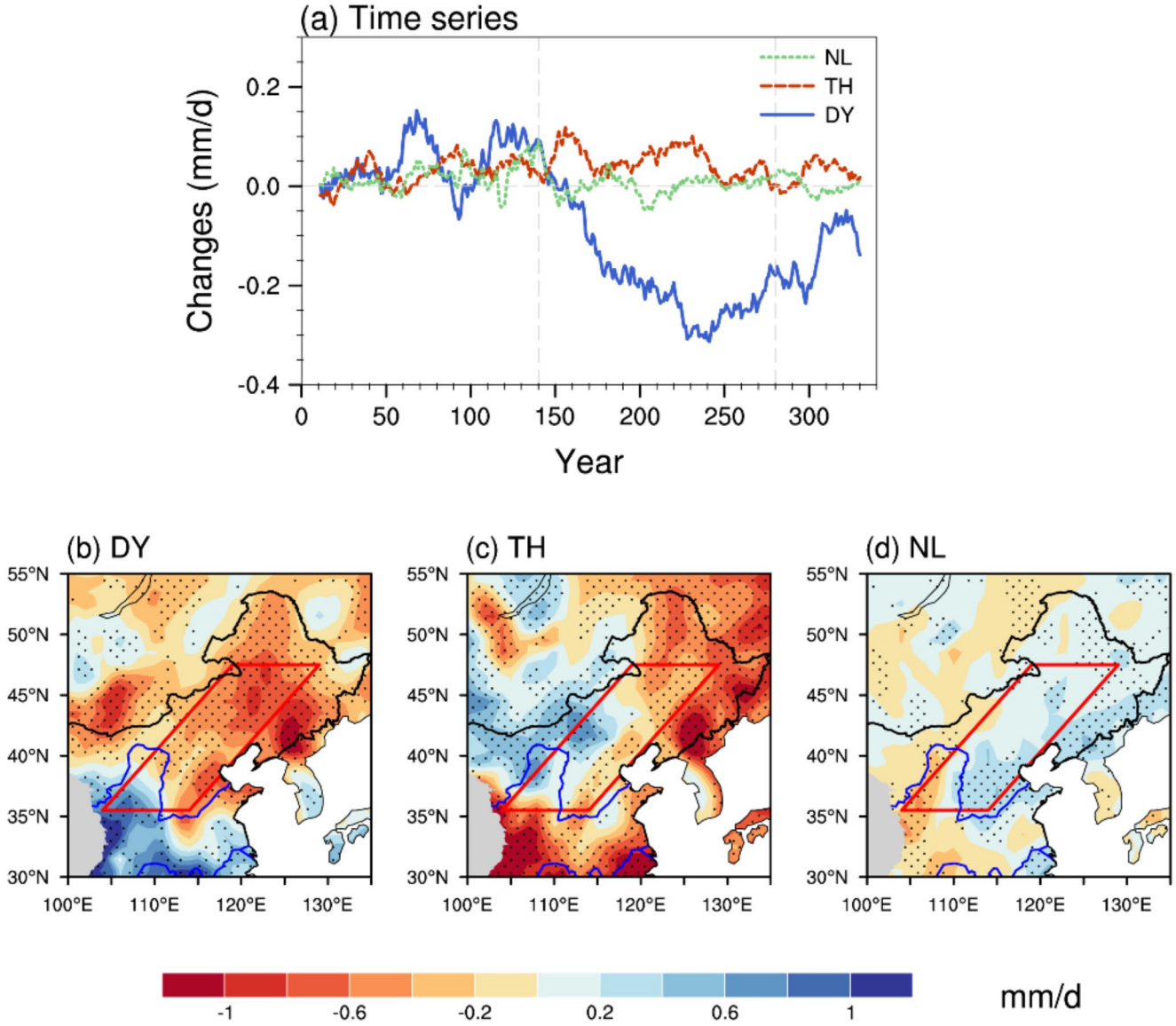

Fig. 5 (**a**) The 21-year running mean changes of dynamic (blue), thermodynamic (red), and nonlinear (green) components (yellow) relative to PI levels in summer in the TCZ. (**b-e**) Spatial differences of dynamic, thermodynamic, and nonlinear components between the CO_2 St and Pk periods (unit: mm·day^{-1}). The stippling and red box are the same as in Fig. 2b

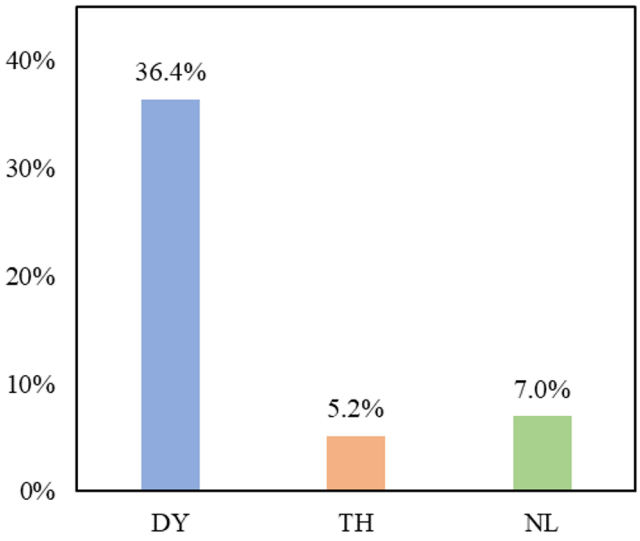

Fig. 6 Coefficients of determination from multiple linear regressions of the dynamic, thermodynamic, and nonlinear components against the P-E changes in TCZ

3.3 Asymmetric response

In addition to examining the differences during the CO_2 stabilization and peak periods, we also observe an obvious asymmetry in the TCZ summer precipitation response (Fig. 7). To investigate the asymmetric change in precipitation, we selected two 20-year time slices (years 61–80 and 239–258; gray bands in Fig. 7), representing periods when the global mean surface temperature increases to 2 °C during CO_2 ramp-up and returns to 2 °C during CO_2 ramp-down. This approach is intended to exclude the influence of delayed global mean surface warming during the CO_2 ramp-down (Zhou et al. 2022). Our analysis reveals that, compared to the CO_2 ramp-up period, the TCZ experiences a notable reduction in summer precipitation during the ramp-down period (Fig. 7b), accompanied by the divergence of the vertically integrated moisture flux (Fig. 7c). Regarding the asymmetry of precipitation, previous studies have typically focused on comparing two-time slices with identical CO_2 concentrations during the CO_2 ramp-up and ramp-down periods (Yeh et al. 2021; Song et al. 2021; Zhang et al. 2023). However, our analysis reveals that, regardless of whether we consider periods of equal temperature increases or equal CO_2 concentrations the TCZ summer precipitation during the CO_2 ramp-down period consistently exhibits a similar reduction compared to the ramp-up period (Fig. S8).

To elucidate the mechanisms driving this asymmetry, we conduct a detailed analysis of moisture transport across the four boundaries of TCZ (Fig. 8). During the CO_2 ramp-down period, while there is a zonal net moisture input of 1.11×10^7 kg·s^{-1}, this is more than offset by a meridional net moisture output of 1.61×10^7 kg·s^{-1}. The combined effect results in a total net moisture output of 0.50×10^7 kg·s^{-1} from the TCZ, leading to widespread moisture divergence and consequently a reduction in precipitation. This imbalance between zonal and meridional moisture transport suggests that the weakening of the summer monsoon circulation during the CO_2 ramp-down period plays a crucial role in modulating the TCZ's moisture budget. Further moisture decomposition analysis (Fig. 9) reveals that the asymmetric response of TCZ summer precipitation is primarily driven by the dynamic component, specifically through the weakening of vertical motion (Fig. S9). The contributions of thermodynamic and nonlinear components are relatively minor, which is consistent with the mechanisms driving the reduction in precipitation during the CO_2 stabilization period compared to the peak period.

These findings highlight that TCZ's hydroclimate may respond differently to future carbon removal scenarios compared to the warming phase. Despite symmetric changes in CO_2 concentrations or global mean temperature, the precipitation response shows a clear asymmetric pattern, with more pronounced drying during the ramp-down period. This asymmetry underscores the complexity of the TCZ's hydroclimatic response, which may diverge significantly under carbon removal strategies. Based on the above results, future research should focus on the differences in the dynamic impacts on the TCZ's hydroclimate during the CO_2 ramp-up and ramp-down periods, which are essential for accurately predicting the region's response to carbon removal strategies and for better assessing the long-term effects on its hydroclimatic stability.

3.4 EASM activity

Based on the findings presented in Sect. 3.2, the meridional moisture transport driven by monsoon circulation plays a more significant role in modulating the summer moisture budget in the TCZ. Therefore, this section further investigates how the moisture budget and precipitation changes in the TCZ are affected by the EASM. Conventionally, quantitative assessments of the EASM have focused primarily on its intensity, with numerous indices proposed to represent it. However, besides EASM intensity, it is equally important to consider the location of the EASM northern boundary and the timing of its impact on the TCZ. Consequently, the impact of the EASM on the TCZ is broadly classified into three aspects: EASM intensity, EASM northern boundary, and EASM influence time.

Based on the EASM intensity index defined by Wang and Fan (1999) (Fig. 10a), the monsoon strengthens during the CO_2 ramp-up period, with a trend of 0.118 m/s/decade. At the initial stage of the CO_2 ramp-down period, the monsoon intensity decreases gradually (trend of -0.075 m/s/decade),

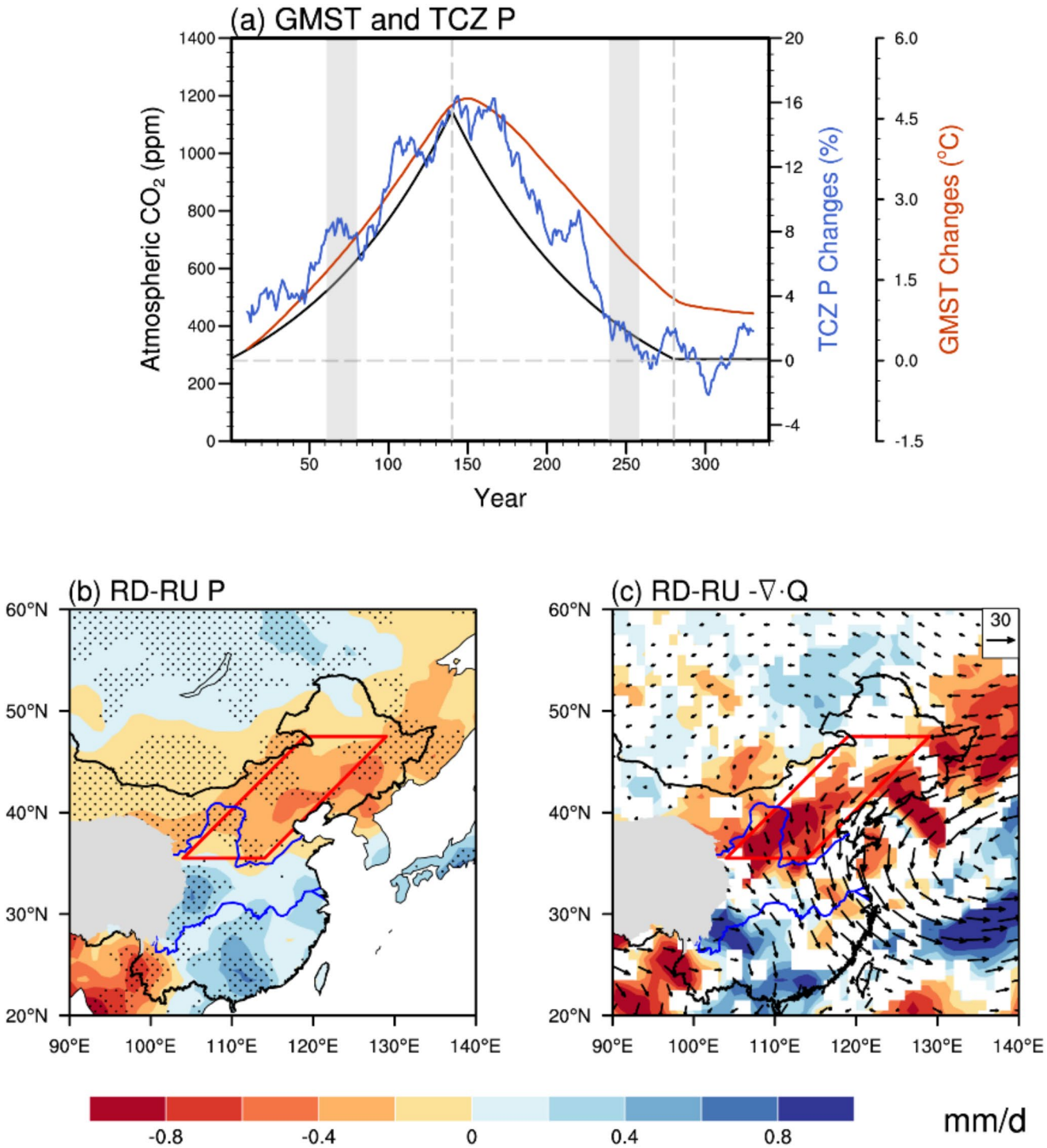

Fig. 7 (**a**) The atmospheric CO_2 concentration (black), the 21-year running mean of global mean surface temperature change (red), and TCZ summer precipitation change (blue) during the CO_2 ramp-up, ramp-down, and stabilization periods relative to the PI levels. The two grey bands covering years 61–80 and 239–258 denote the two representative time slices of 2 °C global mean warming during CO_2 ramp-up and ramp-down. Spatial differences of summer (**b**) precipitation, (**c**) the vertically integrated moisture flux (vectors, unit: $kg \cdot m^{-1} \cdot s^{-1}$) and its divergence (shadings) between CO_2 ramp-down and ramp-up periods (unit: $mm \cdot day^{-1}$)

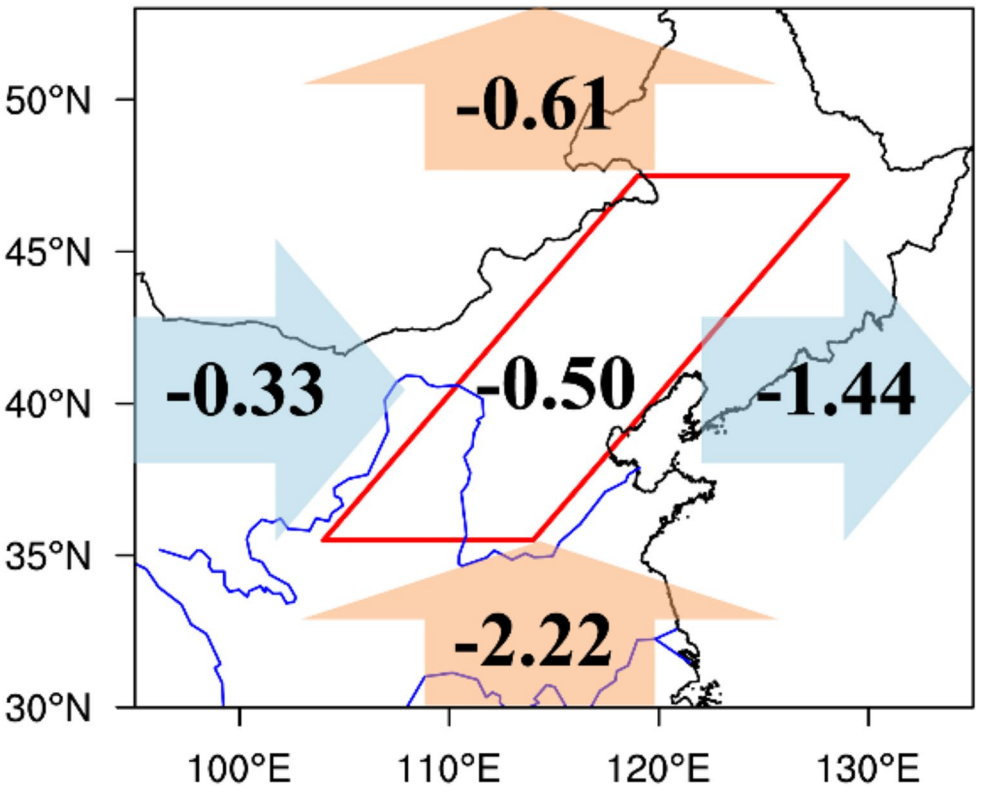

Fig. 8 The same as Fig. 4a, but showing the differences between CO_2 ramp-down and ramp-up periods

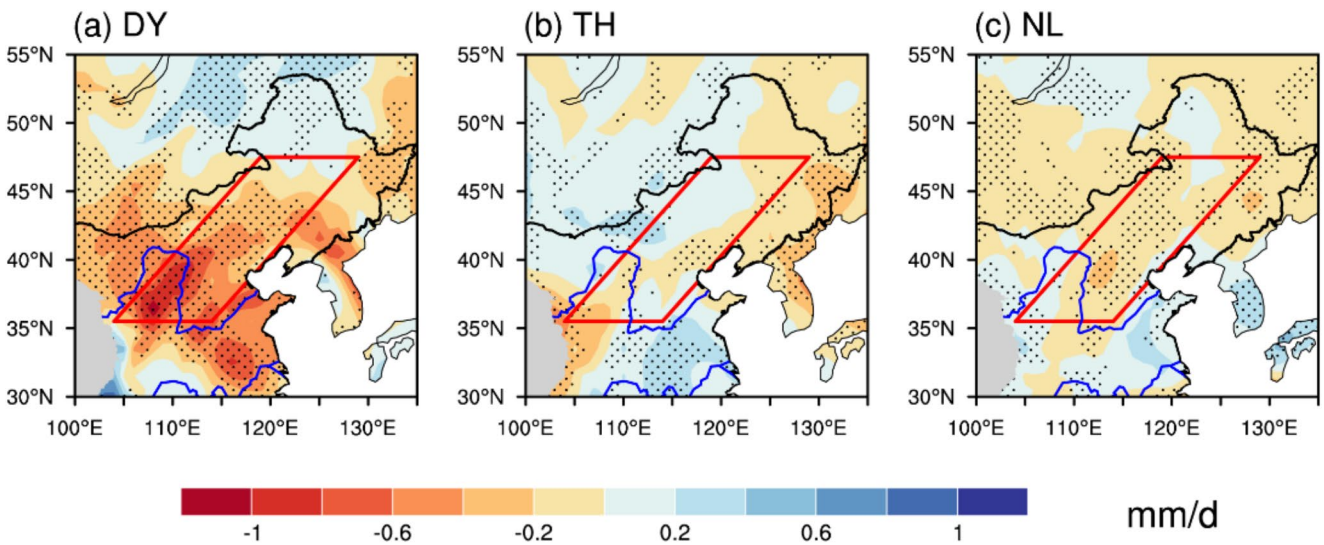

Fig. 9 The same as Fig. 5b-d, but showing the differences between CO_2 ramp-down and ramp-up periods

but it begins to decline more rapidly (trend of -0.306 m/s/decade) around the 240th year. This decrease is not only reflected in the EASM intensity index but is also evident in the reduced precipitation (Fig. S4) and anomalous northeast winds (Fig. S10) in the monsoon region. Furthermore, unlike the precipitation decrease in the TCZ, which is primarily driven by dynamic processes, the reduced precipitation in the monsoon region is predominantly governed by thermodynamic processes (figure not shown). This result is consistent with previous studies on global warming (Zhou et al. 2018, 2020; Moon and Ha 2020). Following the recovery of CO_2 levels, the monsoon intensity also recovers.

Examining the movement of the EASM northern boundary (Fig. 10b), there is a significant northward shift during the CO_2 ramp-up period, consistent with previous studies (Huang et al. 2021; Wang et al. 2022b). As CO_2 levels decrease, the northern boundary retreats rapidly southward, returning to its initial position around the 240th year. It then

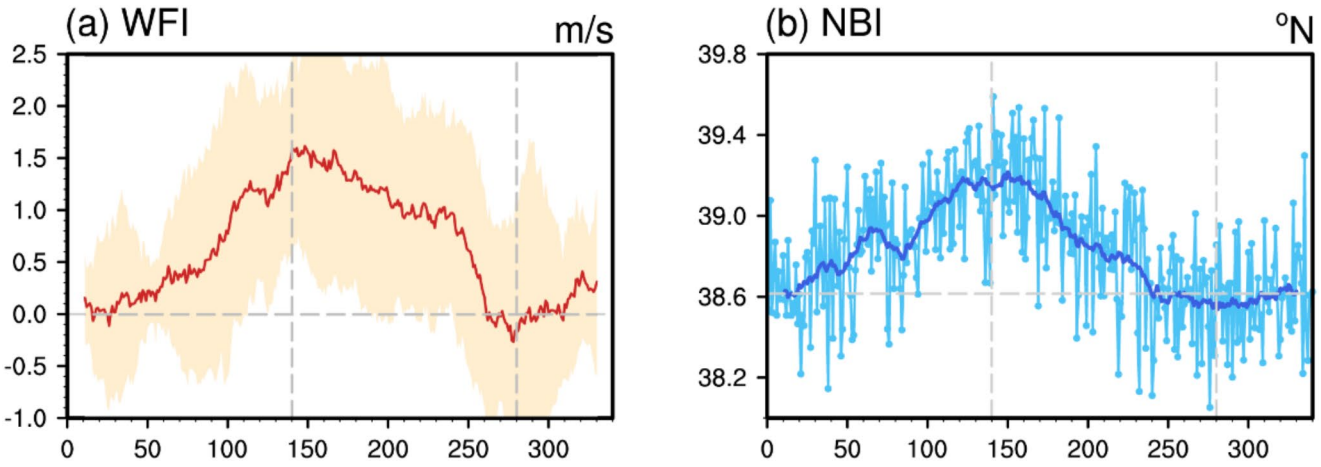

Fig. 10 The 21-year running mean time series of (**a**) the EASM intensity index and (**b**) the EASM northern boundary index during CO_2 ramp-up and ramp-down periods. The shading in (**a**) indicates one standard deviation across the 9 models. The light and dark blue lines in (**b**) indicate interannual and running mean variations, respectively. The dashed vertical lines indicate the CO_2 peak (year 140) and stabilization (year 280) years

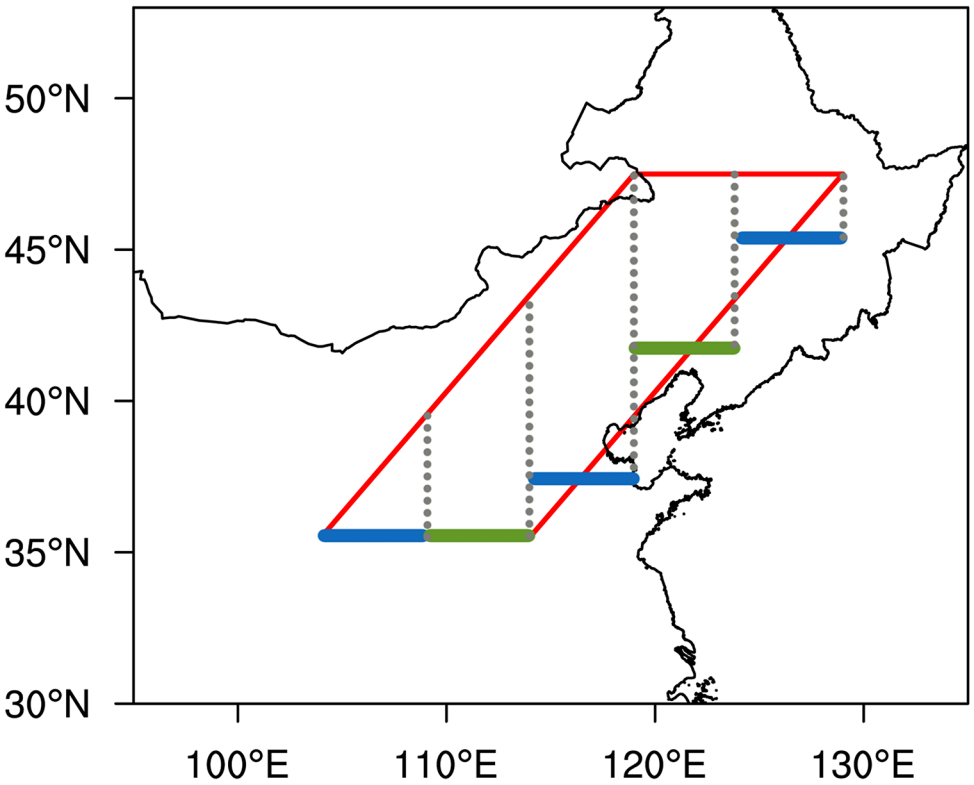

Fig. 11 Boundaries of TCZ (red box) and simplified five segments of TCZ southern boundary (green or blue lines) and their corresponding affected areas (dashed lines). The five segments are 104°E-109°E at 35.5°N, 109°E-114°E at 35.5°N, 114°E-119°E at 37.5°N, 119°E-124°E at 41.5°N, and 124°E-129°E at 45.5°N

continues to retreat slightly until around the 280th year, when it begins to recover, eventually returning to nearly its original position (Fig. S11).

To quantitatively characterize the timing of monsoon influence on the TCZ region, the monsoon rainy onset (MRO), retreat (MRR), and duration (MRD) are analyzed. For convenience, the TCZ is divided into five segments, each spanning five degrees of longitude (Fig. 11): 104°E-109°E at 35.5°N; 109°E-114°E at 35.5°N; 114°E-119°E at 37.5°N; 119°E-124°E at 41.5°N; and 124°E-129°E at 45.5°N. From June to July, the 4 mm day^{-1} precipitation isochrone advances northward, gradually influencing the TCZ, reaching its northernmost extent by late July (highlighted by the thick contour in Fig. 12), which aligns with previous studies. It then retreats southward, withdrawing from the TCZ between August and September (Table S2).

When CO_2 concentration changes, the MRO, MRR, and MRD also vary (Fig. 13). During the pre-industrial,

the southernmost segments (35.5°N) exhibit earlier MRO (mid-June) and a later MRR (mid-September) compared to the northern segments (37.5°N and above), which show later onset (late June) and earlier retreat (late August). This latitudinal variation reflects the decreasing monsoon influence with increasing latitude, resulting in longer duration in southern segments (~100 days) compared to northern ones (~60 days). When CO_2 peaks, the onset advances by up to 15 days and the retreat delays by approximately 6–7 days, leading to an extended rainy season. During the CO_2 removal period, these timing changes show partial recovery but exhibit clear asymmetry, particularly in the MRD: all five segments display overshoot, reflecting the system's hysteresis. While absolute values of MRO, MRR, and MRD may be influenced by model precipitation biases, our analysis focuses on the relative changes across CO_2 change scenarios.

A correlation analysis between the aforementioned EASM activity indices and P-E in the TCZ is conducted, with the results presented in Table 1. The strongest correlation is found with the EASM northern boundary, showing a correlation coefficient of 0.96. Additionally, a strong correlation is observed between P-E and MRD, particularly for the 114°E-119°E, 37.5°N segment (correlation coefficient of 0.91). Averaging the correlation coefficients across the five segments, the values for MRO, MRR, and MRD with respect to P-E are −0.78, 0.80, and 0.83, respectively. The correlation coefficient between EASM intensity and P-E is the lowest with only −0.78. As a result, the EASM northern boundary has the greatest impact on P-E in the TCZ, followed by the EASM influence time, with duration having a greater impact than onset and withdrawal. The least impact comes from the EASM intensity.

4 Summary and discussion

This paper investigates summer precipitation changes in the TCZ under an idealized CO_2 removal simulation. It demonstrates that the TCZ exhibits more pronounced responses to CO_2 forcing due to two key characteristics. First, as a subhumid to semi-arid region, the TCZ receives significantly less precipitation than the monsoon-dominated regions to its south. This relatively low baseline precipitation means that

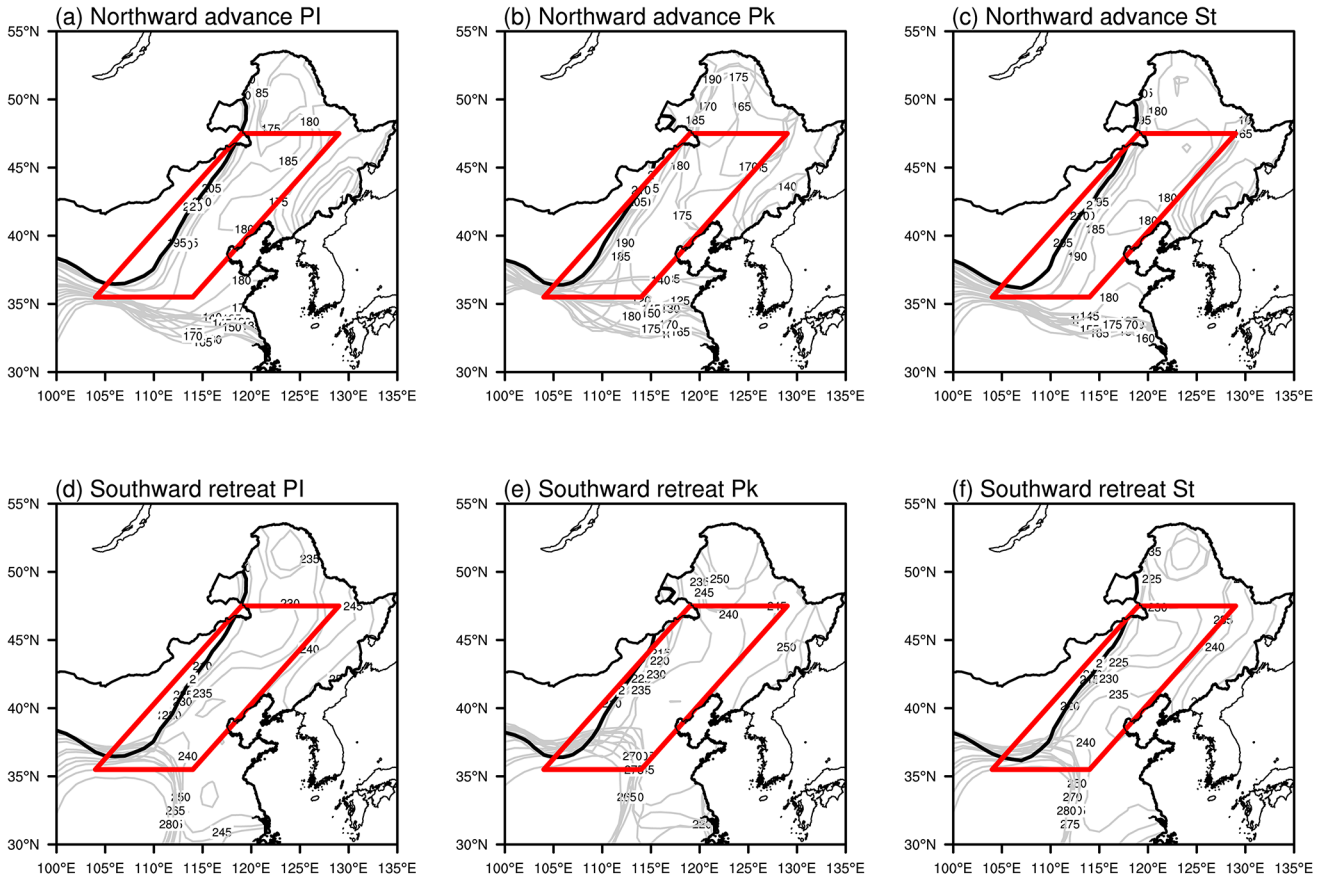

Fig. 12 Dates of the (**a**-**c**) northward advance and (**d**-**f**) southward retreat of the 4 mm d^{-1} isochrones in precipitation (7-day running mean) for the (**a**, **d**) piControl, (**b**, **e**) CO_2 peak, and (**c**, **f**) CO_2 stabilization periods. Contours indicate calendar dates starting from January 1st. Thick contours indicate the 210th day of the year

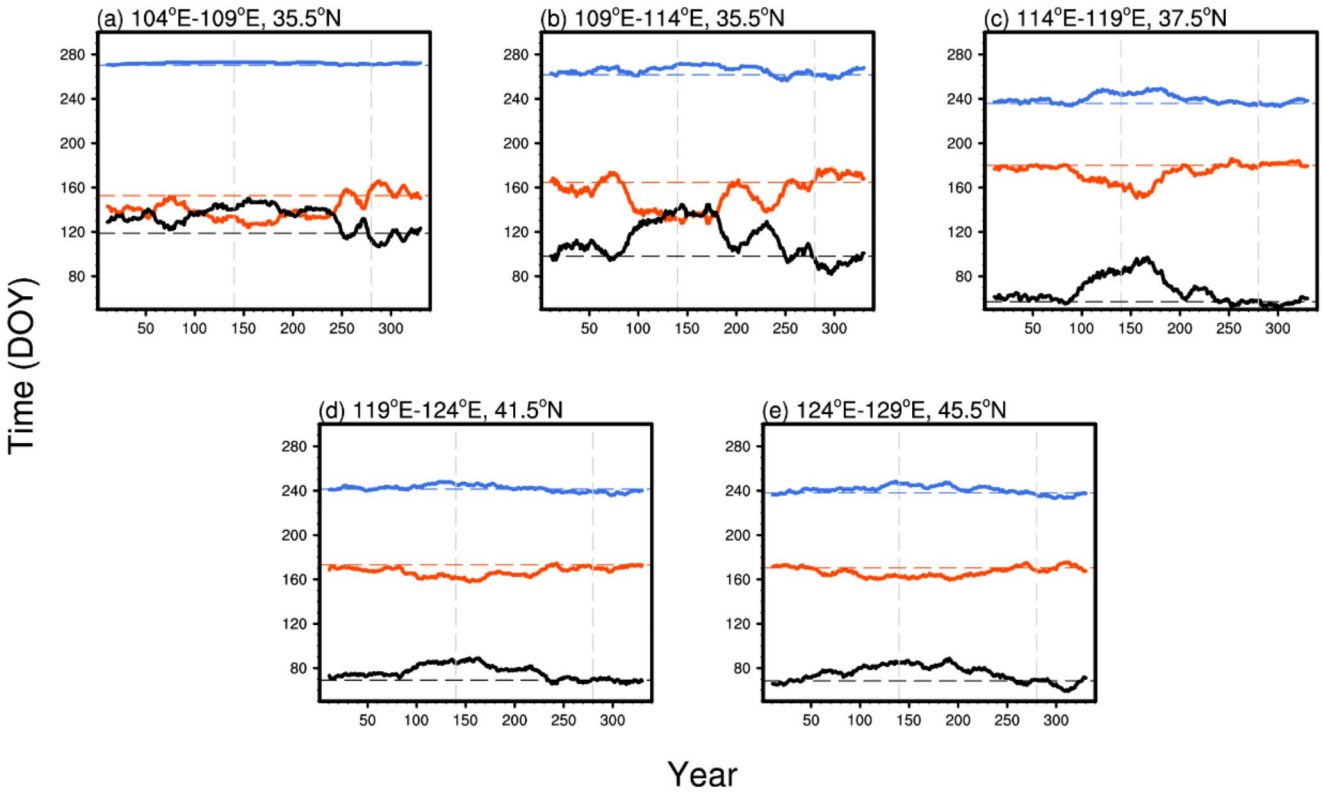

Fig. 13 The 21-year running mean time series of the summer monsoon influencing time over the TCZ. The red, blue, and black solid lines represent the monsoon rainy season onset, retreat, and duration, respectively. The corresponding values in the PI periods are indicated by red, blue, and black horizontal dashed lines. The dashed vertical lines mark the CO_2 peak (year 140) and stabilization (year 280) years

Table 1 Pearson correlation coefficients between precipitation in the TCZ and the EASM activity index. The first numbers in MRO, MRR, and MRD represent the average correlation coefficients of the TCZ's five segments shown in Fig. 11, with ranges shown in brackets. WFI stands for the EASM intensity index, NBI stands for the EASM Northern boundary index, IFT stands for the EASM influence time, and MRO, MRR, and MRD represent the monsoon rainy season onset, retreat, and duration, respectively

WFI	NBI	IFT		
		MRO	MRR	MRD
0.78	0.96	-0.78 (-0.71∼-0.87)	0.80 (0.72∼0.89)	0.83 (0.73∼0.89)

even moderate absolute changes can result in large percentage variations. Second, unlike the arid regions to its north that are beyond monsoon influence, the TCZ is situated at the northern margin of the EASM. This location makes it particularly susceptible to monsoon variability, which often induces substantial precipitation changes.

During the CO_2 ramp-up period, precipitation increases across the region, reaching a 15% increase relative to PI levels at the CO_2 peak, and remains elevated for about 20 years. Following this, precipitation in the TCZ decreases in line with CO_2 removal. Notably, the asymmetry in summer precipitation during the CO_2 ramp-up and ramp-down periods is evident, with the TCZ experiencing a pronounced reduction in precipitation during the ramp-down period, despite reaching the same global mean surface temperature.

According to moisture budget diagnoses, it is found that a reduction in P-E across the TCZ during the CO_2 ramp-down period, particularly in the northeastern areas, corresponding with the divergence of vertically integrated atmospheric moisture flux with a correlation coefficient of -0.67. Further decomposition reveals that the dynamic component, related to wind field anomalies and demonstrating the strongest robustness, contributes the most to the P-E change, accounting for 36.4%. The thermodynamic and nonlinear components contribute 5.2% and 7.0%, respectively. Meanwhile, the dynamic component is also the primary factor for the asymmetric response of TCZ summer precipitation under the condition of the same global-mean temperature increase during both CO_2 ramp-up and ramp-down periods. Given that the TCZ is influenced by both the westerlies and the monsoon, we analyze moisture transport into the TCZ through four boundaries and assess the total moisture budget. During the CO_2 ramp-down period, the TCZ experiences a net moisture output of 0.16×10^7 kg·s^{-1}, composed of a zonal net input of 2.32×10^7 kg·s^{-1} and a meridional net output of 2.48×10^7 kg·s^{-1}. The zonal and meridional moisture transport contribute to changes in vertically integrated

water vapor flux divergence by 18.3% and 78.6%, respectively, indicating that the monsoon primarily drives summer net moisture budget changes in the TCZ.

The impact of the monsoon can be assessed through various aspects: EASM intensity, EASM northern boundary, and EASM influence times, including onset, retreat, and duration. During the CO_2 ramp-up period, the EASM shows a strengthening intensity, a significant northward movement of the northern boundary, and earlier onset, later retreat, and longer duration of the monsoon rainy season. Conversely, during the CO_2 ramp-down period, the EASM shows a weakening intensity, a significant southward retreat of the northern boundary, and later onset, earlier retreat, and shorter duration of the monsoon rainy season. Among these factors, the EASM northern boundary exhibits the greatest impact on the P-E decrease, with a correlation coefficient of 0.96, followed by the EASM influence time. The EASM intensity has the least impact.

In conclusion, this research comprehensively investigates the TCZ precipitation response to CO_2 removal, revealing several novel findings: (1) despite equivalent global warming levels, TCZ summer precipitation is lower during CO_2 ramp-down than ramp-up phases, highlighting its asymmetric response; the dynamic component contributes more significantly to precipitation changes (36.4%) than the thermodynamic component (5.2%) throughout CO_2 evolution; (3) the identification of distinct EASM characteristics affecting TCZ precipitation during CO_2 changing, with the northern boundary shift showing the strongest impact. These insights advance our understanding of regional climate response to CO_2 removal scenarios and have important implications for future climate adaptation strategies.

Supplementary Information The online version contains supplementary material available at https://doi.org/10.1007/s00382-025-07647-2.

Acknowledgements We thank the editor and the two anonymous referees for their valuable comments that helped to improve the manuscript.

Funding This work was supported by the National Natural Science Foundation of China (Grants Nos. 42175041, 42141019 and 42375044), the International Partnership Program of Chinese Academy of Sciences for Future Network (Grant No. 060GJHZ2022104FN), and the Youth Program of the Institute of Atmospheric Physics, Chinese Academy of Sciences during the 14th Five-Year Plan Period.

Data availability The daily observation precipitation data used in this study is provided by the National Meteorological Information Center of the China Meteorological Administration (CMA; https://data.cma.cn/). The PREC/L data were downloaded from NOAA/PSL: https://psl.noaa.gov/data/gridded/data.gpcc.html. CRU TS4.07 precipitation: https://data.ceda.ac.uk/badc/cru/data/cru_ts/cru_ts_4.07/data/pre. The CMIP6 outputs are available online at https://esgf-node.llnl.gov/search/cmip6/.

Declarations

Competing interests The authors have no relevant financial or non-financial interests to disclose.

References

Bueh C, Li Y, Lin D, Lian Y (2016) Interannual variability of summer rainfall over the Northern part of China and the related circulation features. J Meteorol Res 30:615–630. https://doi.org/10.1007/s13351-016-5111-5

Cao L, Jin X-Y, Jiang J (2023) Simulated carbon cycle and Earth system response to atmospheric CO2 removal. Adv Clim Change Res 14:313–321. https://doi.org/10.1016/j.accre.2023.03.001

Chen H, Sun J (2015) Changes in drought characteristics over China using the standardized precipitation evapotranspiration index. J Clim 28:5430–5447. https://doi.org/10.1175/JCLI-D-14-00707.1

Chen M, Xie P, Janowiak JE, Arkin PA (2002) Global land precipitation: A 50-yr monthly analysis based on gauge observations. J Hydrometeorol 3:249–266. https://doi.org/10.1175/1525-7541(2002)003%3C0249:GLPAYM%3E2.0.CO;2

Chen J, Huang W, Jin L et al (2018) A Climatological Northern boundary index for the East Asian summer monsoon and its interannual variability. Sci China Earth Sci 61:13–22. https://doi.org/10.1007/s11430-017-9122-x

Chen W, Wang L, Feng J et al (2019) Recent progress in studies of the variabilities and mechanisms of the East Asian monsoon in a changing climate. Adv Atmos Sci 36:887–901. https://doi.org/10.1007/s00376-019-8230-y

Chen W, Zhang R, Wu R et al (2023) Recent advances in Understanding Multi-scale climate variability of the Asian monsoon. Adv Atmos Sci 40:1429–1456. https://doi.org/10.1007/s00376-023-2266-8

Chen W, Piao J, Chen S et al (2024) Multi-Scale variations and future projections of Dry-Wet conditions over the monsoon transitional zone in East Asia: A review. https://doi.org/10.1016/j.fmre.2024.01.023. Fundamental Research

Ha K-J, Moon S, Timmermann A, Kim D (2020) Future changes of summer monsoon characteristics and evaporative demand over Asia in CMIP6 simulations. Geophys Res Lett 47. https://doi.org/10.1029/2020GL087492. e2020GL087492

Harris I, Osborn TJ, Jones P, Lister D (2020) Version 4 of the CRU TS monthly high-resolution gridded multivariate climate dataset. Sci Data 7:109. https://doi.org/10.1038/s41597-020-0453-3

Hou H, Qu X, Huang G (2021) Reversal asymmetry of rainfall change over the Indian ocean during the radiative forcing increase and stabilization. Earth's Future 9. https://doi.org/10.1029/2021EF002272. e2021EF002272

Huang X, Yang S, Haywood A et al (2021) Warming-Induced Northwestward migration of the Asian summer monsoon in the geological past: evidence from climate simulations and geological reconstructions. J Geophys Research: Atmos. https://doi.org/10.1029/2021JD035190. 126:e2021JD035190

Huang G, Xu Z, Qu X et al (2022) Critical climate issues toward carbon neutrality targets. Fundamental Res 2:396–400. https://doi.org/10.1016/j.fmre.2022.02.011

Jo S-Y, Seong M-G, Min S-K et al (2022) Hysteresis behaviors in East Asian extreme precipitation frequency to CO2 pathway. Geophys Res Lett 49. https://doi.org/10.1029/2022GL099814. e2022GL099814

Keller DP, Lenton A, Scott V et al (2018) The carbon dioxide removal model intercomparison project (CDRMIP): rationale and

experimental protocol for CMIP6. Geosci Model Dev 11:1133–1160. https://doi.org/10.5194/gmd-11-1133-2018
Lin Z (2014) Intercomparison of the impacts of four summer teleconnections over Eurasia on East Asian rainfall. Adv Atmos Sci 31:1366–1376. https://doi.org/10.1007/s00376-014-3171-y
Lin Z, Wang B (2016) Northern East Asian low and its impact on the interannual variation of East Asian summer rainfall. Clim Dyn 46:83–97. https://doi.org/10.1007/s00382-015-2570-9
Long S-M, Xie S-P, Du Y et al (2020) Effects of ocean slow response under low warming targets. J Clim 33:477–496. https://doi.org/10.1175/JCLI-D-19-0213.1
Lu W, Jia G (2013) Fluctuation of farming-pastoral ecotone in association with changing East Asia monsoon climate. Clim Change 119:747–760. https://doi.org/10.1007/s10584-013-0761-0
Ma Z, Fu C (2006) Some evidence of drying trend over Northern China from 1951 to 2004. Chin SCI BULL 51:2913–2925. https://doi.org/10.1007/s11434-006-2159-0
Moon S, Ha K-J (2020) Future changes in monsoon duration and precipitation using CMIP6. Npj Clim Atmos Sci 3:1–7. https://doi.org/10.1038/s41612-020-00151-w
Neilson RP (1993) Transient ecotone response to Climatic change: some conceptual and modelling approaches. Ecol Appl 3:385–395. https://doi.org/10.2307/1941907
Piao J, Chen W, Wei K et al (2017) An abrupt rainfall decrease over the Asian inland plateau region around 1999 and the possible underlying mechanism. Adv Atmos Sci 34:456–468. https://doi.org/10.1007/s00376-016-6136-5
Piao J, Chen W, Chen S (2021a) Water vapour transport changes associated with the interdecadal decrease in the summer rainfall over Northeast Asia around the late-1990s. Int J Climatol 41:E1469–E1482. https://doi.org/10.1002/joc.6780
Piao J, Chen W, Chen S et al (2021b) Mean States and future projections of precipitation over the monsoon transitional zone in China in CMIP5 and CMIP6 models. Clim Change 169:35. https://doi.org/10.1007/s10584-021-03286-8
Piao J, Chen W, Wang L, Chen S (2022) Future projections of precipitation, surface temperatures and drought events over the monsoon transitional zone in China from bias-corrected CMIP6 models. Int J Climatol 42:1203–1219. https://doi.org/10.1002/joc.7297
Piao J, Chen W, Chen S et al (2023) How well do CMIP6 models simulate the Climatological Northern boundary of the East Asian summer monsoon? Glob Planet Change 221:104034. https://doi.org/10.1016/j.gloplacha.2023.104034
Qian WH, Qin A (2008) Precipitation division and climate shift in China from 1960 to 2000. Theor Appl Climatol 93:1–17. https://doi.org/10.1007/s00704-007-0330-4
Ren Z, Chen W, Wang L et al (2024) Comparative analysis of East Asian summer monsoon Northern boundary indices: variability, climate anomalies and driving mechanisms. Clim Dyn 63:35. https://doi.org/10.1007/s00382-024-07526-2
Shi Z (1996) Regional characters of natural disaster in marginal monsoon belt of China. J Arid Land Resour Environ 10:1–7 (in Chinese)
Simmonds I, Bi D, Hope P (1999) Atmospheric water vapor flux and its association with rainfall OverChina in summer. J Clim 12:1353–1367. https://doi.org/10.1175/1520-0442(1999)012%3C1353:AWVFAI%3E2.0.CO;2
Song S-Y, Yeh S-W, An S-I et al (2021) Asymmetrical response of summer rainfall in East Asia to CO2 forcing. Sci Bull S209592732100596X. https://doi.org/10.1016/j.scib.2021.08.013
Su X, Huang G, Wang L, Wang T (2024) Global drought changes and attribution under carbon neutrality scenario. Clim Dyn 1–18. https://doi.org/10.1007/s00382-024-07310-2
Sun M-A, Sung HM, Kim J et al (2021) Reversibility of the hydrological response in East Asia from CO2-derived climate change based on CMIP6 simulation. Atmosphere 12. https://doi.org/10.3390/atmos12010072
Tang X, Qian W, Liang P (2006) Climatic features of boundary belt for East Asia summer monsoon. Plateau Meteorol 25:375–381 (in Chinese)
Trenberth KE, Guillemot CJ (1995) Evaluation of the global atmospheric moisture budget as seen from analyses. J Clim 8:2255–2272. https://doi.org/10.1175/1520-0442(1995)008%3C2255:EOTGAM%3E2.0.CO;2
Tu C, Huang S (1944) The advance and withdraw of East Asia summer monsoon. Acta Meteorologica Sinica 18:1–20 (in Chinese)
Wang H (2002) The instability of the East Asian summer monsoon–ENSO relations. Adv Atmos Sci 19:1–11. https://doi.org/10.1007/s00376-002-0029-5
Wang B, Fan Z (1999) Choice of South Asian summer monsoon indices. Bull Am Meteorol Soc 80:629–638. https://doi.org/10.1175/1520-0477(1999)080%3C0629:COSASM%3E2.0.CO;2
Wang H, He S (2015) The North China/Northeastern Asia severe summer drought in 2014. J Clim 28:6667–6681. https://doi.org/10.1175/JCLI-D-15-0202.1
Wang B, LinHo (2002) Rainy season of the Asian–Pacific summer monsoon. J Clim 15:386–398. https://doi.org/10.1175/1520-0442(2002)015%3C0386:RSOTAP%3E2.0.CO;2
Wang A, Wu C, Lin W et al (1999) The definition of the advance and retreat of the summer monsoon in China. Plateau Meteorol 18:400–408 (in Chinese)
Wang B, Wu Z, Li J et al (2008) How to measure the strength of the East Asian summer monsoon. J Clim 21:4449–4463. https://doi.org/10.1175/2008JCLI2183.1
Wang L, Chen W, Huang G, Zeng G (2017) Changes of the transitional climate zone in East Asia: past and future. Clim Dyn 49:1463–1477. https://doi.org/10.1007/s00382-016-3400-4
Wang Q, Wang L, Huang G et al (2021) Temporal and Spatial variation of the transitional climate zone in summer during 1961–2018. Int J Climatol 41:1633–1648. https://doi.org/10.1002/joc.6902
Wang Q, Wang L, Huang G, Wang T (2022a) Mechanism of the summer rainfall interannual variability in transitional climate zone in East Asia: roles of teleconnection patterns and associated moisture processes. Clim Dyn. https://doi.org/10.1007/s00382-022-06618-1
Wang Z, Fu Z, Liu B et al (2022b) Northward migration of the East Asian summer monsoon Northern boundary during the twenty–first century. Scientific Reports
Wang L, Huang G, Chen W, Wang T (2023a) Super drought under global warming: concept, monitoring index, and validation. Bull Am Meteorol Soc 104:E943–E969. https://doi.org/10.1175/BAMS-D-22-0182.1
Wang Q, Huang G, Wang L et al (2023b) Mechanism of the summer rainfall variation in transitional climate zone in East Asia from the perspective of moisture supply during 1979–2010 based on the lagrangian method. Clim Dyn 60:1225–1238. https://doi.org/10.1007/s00382-022-06344-8
Wu C, Liu H, Xie A (2005) Interdecadal characteristics of the influence of northward shift and intensity of summer monsoon on precipitation over Northern China in summer. Plateau Meteorol 24:656–665 (in Chinese)
Wu P, Ridley J, Pardaens A et al (2015) The reversibility of CO2 induced climate change. Clim Dyn 45:745–754. https://doi.org/10.1007/s00382-014-2302-6
Xu Y, Zhao P, Si D et al (2020) Development and preliminary application of a gridded surface air temperature homogenized dataset for China. Theor Appl Climatol 139:505–516. https://doi.org/10.1007/s00704-019-02972-z
Yeh S-W, Song S-Y, Allan RP et al (2021) Contrasting response of hydrological cycle over land and ocean to a changing CO2

pathway. Npj Clim Atmospheric Sci 4. https://doi.org/10.1038/s41612-021-00206-6

Zhang S, Qu X, Huang G, Hu P (2023) Asymmetric response of South Asian summer monsoon rainfall in a carbon dioxide removal scenario. Npj Clim Atmos Sci 6:10. https://doi.org/10.1038/s41612-023-00338-x

Zhao G, Huang G, Wu R et al (2015) A new Upper-Level circulation index for the East Asian summer monsoon variability. J Clim 28:9977–9996. https://doi.org/10.1175/JCLI-D-15-0272.1

Zhao W, Chen S, Chen W et al (2019a) Interannual variations of the rainy season withdrawal of the monsoon transitional zone in China. Clim Dyn 53:2031–2046. https://doi.org/10.1007/s00382-019-04762-9

Zhao W, Chen S, Chen W et al (2019b) Interannual variations of the rainy season withdrawal of the monsoon transitional zone in China. Clim Dyn 53:2031–2046. https://doi.org/10.1007/s00382-019-04762-9

Zhao W, Chen W, Chen S et al (2019c) Inter-annual variations of precipitation over the monsoon transitional zone in China during August-September: role of sea surface temperature anomalies over the tropical Pacific and North Atlantic. Atmos Sci Lett 20:e872. https://doi.org/10.1002/asl.872

Zhao W, Chen W, Chen S et al (2020) Combined impact of tropical central-eastern Pacific and North Atlantic sea surface temperature on precipitation variation in monsoon transitional zone over China during August–September. Int J Climatol 40:1316–1327. https://doi.org/10.1002/joc.6231

Zhou X, Lu R (2024) The unprecedented extreme anticyclonic anomaly over Northeast Asia in July 2021 and its Climatic impacts. Adv Atmos Sci 41:608–618. https://doi.org/10.1007/s00376-023-3026-5

Zhou S, Huang G, Huang P (2018) Changes in the East Asian summer monsoon rainfall under global warming: moisture budget decompositions and the sources of uncertainty. Clim Dyn 51:1363–1373. https://doi.org/10.1007/s00382-017-3959-4

Zhou S, Huang G, Huang P (2020) A bias-corrected projection for the changes in East Asian summer monsoon rainfall under global warming. Clim Dyn 54:1–16. https://doi.org/10.1007/s00382-019-04980-1

Zhou S, Huang P, Xie S-P et al (2022) Varying contributions of fast and slow responses cause asymmetric tropical rainfall change between CO2 ramp-up and ramp-down. Sci Bull. https://doi.org/10.1016/j.scib.2022.07.010